

Geophysical Research Letters®

RESEARCH LETTER

10.1029/2022GL097989

Key Points:

- Via a 1-D gcPIC- δf simulation in a dipole field, we have investigated the repetitive chorus emissions excited by anisotropic electrons
- Two of the chorus elements have rising frequency chirpings, mingled with one element with a hooked-tone structure
- Along with the generation of both rising-tone and hooked-tone chorus elements, there are clear electron holes in the $v_{||}$ - ζ plane

Correspondence to:

Q. Lu and X. Wang,
qmlu@ustc.edu.cn;
xywang@physics.auburn.edu

Citation:

Chen, H., Lu, Q., Wang, X., Fan, K., Chen, R., & Gao, X. (2022). One-dimensional gcPIC- δf simulation of hooked chorus waves in the Earth's inner magnetosphere. *Geophysical Research Letters*, 49, e2022GL097989. <https://doi.org/10.1029/2022GL097989>

Received 24 JAN 2022
 Accepted 6 FEB 2022

One-Dimensional gcPIC- δf Simulation of Hooked Chorus Waves in the Earth's Inner Magnetosphere

Huayue Chen^{1,2} , Quanming Lu^{1,2} , Xueyi Wang³ , Kai Fan^{1,2} , Rui Chen^{1,2} , and Xinliang Gao^{1,2} 

¹Department of Geophysics and Planetary Science, CAS Key Laboratory of Geospace Environment, University of Science and Technology of China, Hefei, China, ²CAS Center for Excellence in Comparative Planetology, Hefei, China, ³Department of Physics, Auburn University, Auburn, AL, USA

Abstract Chorus waves are coherent electromagnetic emissions in the inner magnetosphere, generally composed of a series of discrete and repetitive elements. These elements usually have rising frequency chirpings, which are occasionally mingled with one or several elements with a hooked spectrogram. In this letter, we perform a one-dimensional general curvilinear particle-in-cell (gcPIC)- δf simulation of chorus waves excited by temperature anisotropic electrons in a dipole magnetic field, and identify one chorus element with a hooked spectrogram, which is embedded in several chorus elements with a rising frequency chirping. In the hooked chorus element, the frequency increases first, and then decreases. Interestingly, we find that there are clear electron holes in the electron velocity space, no matter whether the chorus element has a rising-tone or hooked-tone spectrogram. Our study presents an important clue for the theoretical analysis of the frequency chirping in the chorus waves.

Plain Language Summary Chorus waves are intense electromagnetic emissions that occur naturally in the Earth's inner magnetosphere, which usually contain a series of discrete chirping elements. Via a one-dimensional (1-D) general curvilinear particle-in-cell (gcPIC)- δf simulation in a dipole field, we have investigated the frequency chirping of chorus waves, excited by anisotropic electrons. After the waves leave away from the equator, their frequencies chirp, exhibiting as quasi-monochromatic emissions. Together with two rising-tone elements, there is one element with a hooked spectrogram, whose frequency first increases, and then decreases. This is consistent with the satellite observation of hooked-tone elements. In the $v_{||}$ - ζ plane, there are clear electron holes along with both rising-tone and hooked-tone chorus elements. Our study provides a novel idea for the theoretical work of chorus frequency chirping.

1. Introduction

As one of the most commonly observed plasma waves in the Earth's inner magnetosphere, whistler-mode waves play an important role in governing electron dynamics therein (Burtis & Helliwell, 1969; Horne & Thorne, 1998; Horne et al., 2003; Tsurutani & Smith, 1974). They can not only produce relativistic electrons in the radiation belt (Meredith et al., 2001; Summers et al., 1998), but also lead to electron precipitation into the Earth's upper atmosphere (Lorentzen et al., 2001; Nishimura et al., 2013; Thorne et al., 2010). Whistler-mode waves are considered to be excited around the magnetic equator by energetic electrons injected from the magnetotail, which typically have the temperature anisotropy with $T_{\perp} > T_{\parallel}$ (T_{\perp} and T_{\parallel} are the perpendicular and parallel temperatures concerning the background magnetic field) (Chen et al., 2017, 2021; Kennel & Petschek, 1966; Q. M. Lu et al., 2004; Santolík & Gurnett, 2003; Tsurutani & Smith, 1977). When these waves leave away from the source region around the magnetic equator, they usually evolve into chorus waves with a narrowband spectrum, which may exhibit rising, falling, or hooked tones (Helliwell, 1967; Pickett et al., 2005; Tsurutani & Smith, 1974). In general, the chorus waves with a rising tone are much more often observed than other kinds of spectrograms (Nunn et al., 1997). Satellite observations have shown that among the rising elements, there are occasionally one or several elements with a hooked spectrogram. Figure 1 presents three chorus wave events captured by Van Allen Probes-A, which all contain several quasi-parallel propagating rising-tone and hooked-tone (whose spectrogram exhibits as flat or downward chirping after the peak frequency) elements. The similar spectrograms have also been reported and described in detail in the previous work (Turner et al., 2017). The repetitive appearance of chorus elements is considered to be related to the injected energetic electrons (Q. Lu et al., 2021). Nevertheless, the formation of frequency chirping has not been fully understood yet.

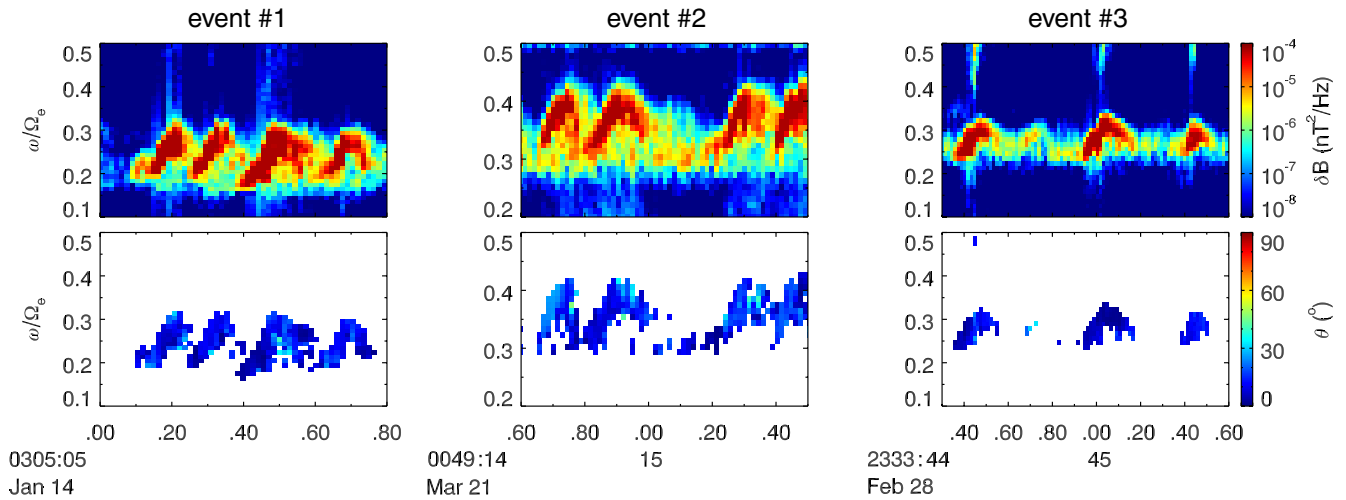


Figure 1. Three chorus chirping events captured by Van Allen Probe A at $L = 5-6$, in which the top row represents the spectrograms of magnetic power, and the bottom row shows the wave normal angles.

Numerous particle-in-cell (PIC) and Vlasov simulations have been dedicated to studying chorus waves in the Earth's inner magnetosphere (Hikishima et al., 2009; Katoh & Omura, 2011; Ke et al., 2017, 2020; Nunn et al., 1997; Nunn & Omura, 2012; Q. Lu et al., 2019, 2021; Tao, 2014, 2017). Chorus waves with rising, falling, and hooked tones have been reproduced in one-dimensional (1-D) Vlasov simulations with the ambient magnetic field close to being a parabolic function of the distance from the equator, where the monochromatic whistler-mode wave is injected into the system as a pump wave (Nunn & Omura, 2012; Nunn et al., 1997). Rising-tone chorus waves have also been simulated in 1-D PIC simulations with the same ambient magnetic field (Hikishima et al., 2009; Tao, 2014, 2017), as well as in two-dimensional (2-D) PIC simulations in a dipole magnetic field (Q. Lu et al., 2019). The rising-tone chorus waves are considered to be associated with an electron hole in the wave phase space and negative resonance current, which is formed due to the nonlinear trapping of resonant electrons by the whistler-mode waves (Nunn, 1974; Omura et al., 2008). While, falling-tone chorus waves are believed to be associated with an electron hill and positive resonance current (Nunn & Omura, 2012; Omura et al., 2015). Then, what kind of structure in the electron phase space is formed in hooked chorus waves becomes a puzzle. In this letter, with the 1-D general curvilinear particle-in-cell (gcPIC) δf simulation model, we at first reproduce chorus waves with a hooked tone in the dipole magnetic field, and then the associated structure in the electron phase space is characterized in detail.

2. Simulation Model and Initial Setup

To investigate the frequency chirping in chorus waves, we adopt the 1-D gcPIC- δf simulation model in a dipole magnetic field. The δf method is a low-noise technology (Hu & Krommes, 1994; Parker & Lee, 1993; Sydora, 2003; Tao et al., 2017), in which the full particle velocity distribution f can be divided into $f = f_0 + \delta f$ (where f_0 is the equilibrium distribution), and the perturbed distribution function δf will be updated. Compared with conventional PIC simulations, the δf method can significantly reduce the noise level by calculating δf directly from particles (Q. Lu et al., 2021; Sydora, 2003; Tao et al., 2017). In our study, the absorbing boundary is applied for electromagnetic fields, while the reflecting boundary condition has been employed for particles. There are two electron components: cold and energetic electrons, which are all moving in the motion of Lorentz force. Especially, the energetic electrons are injected continuously into the system due to an azimuthal drift. Because of $\omega \gg \Omega_i$ (where ω is the wave frequency and Ω_i is the ion gyrofrequency), the ions are assumed to be motionless. Other details of this model can be found in Q. Lu et al. (2021).

Initially, the energetic electrons satisfy a bi-Maxwellian distribution. The temperature anisotropy and number density of the energetic electrons at the equator are $T_{\perp eq}/T_{\parallel eq} = 6$ and $n_{heq}/n_{co} = 0.006$ (where n_{co} is the number density of cold electrons, which is assumed to be uniformly distributed in the simulation domain), and the parallel plasma beta of energetic electrons is $\beta_{\parallel h0} = n_{h0}T_{\parallel 0}/(B_{0eq}^2/2\mu_0) = 0.001$ (corresponds to the parallel thermal

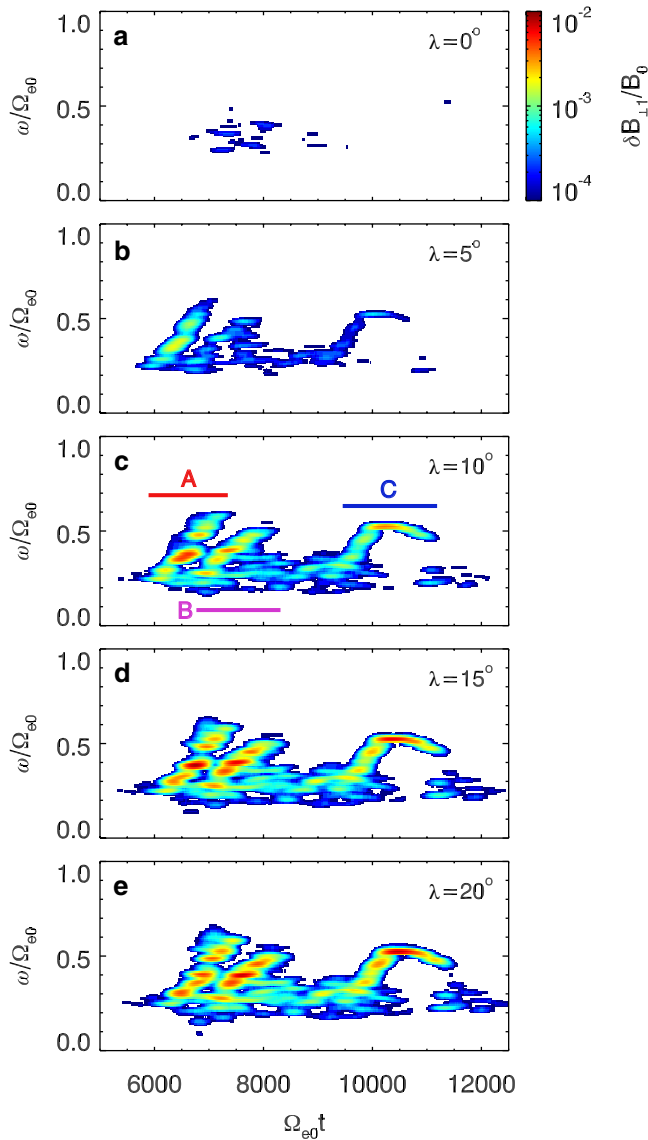


Figure 2. The ω - t spectrogram of $\delta B_{\perp 1}$ at the latitude of λ =(a) 0° , (b) 5° , (c) 10° , (d) 15° , and (e) 20° . The three chirping elements have been denoted by the three segments in different colors in panel (c).

velocity $v_{\text{th}}/V_{Ae} = 0.442$, where V_{Ae} is the electron Alfvén speed). The electron distributions along the magnetic field can be obtained with Liouville's theorem (Summers et al., 2012). The ratio of cold electron plasma frequency to electron gyrofrequency is $\omega_{pe}/\Omega_{e0} = 5.0$ (where $\omega_{pe} = \sqrt{n_{e0}e^2/m_e\epsilon_0}$ and $\Omega_{e0} = eB_0/m_e$ are defined on the background magnetic field B_0 at the equator). These are typical values at the L-shell around 6. However, to save computational source, the topology of the magnetic field in the simulations is roughly equal to that at $L = 0.5$. The latitude ranges from about -27.6° to 27.6° . We use 4,000 cells in total, with the cell length of $0.34d_e$ (where $d_e = c/\omega_{pe}$ is the electron inertial length). There are about 4,000 particles per cell on average. The energetic electrons with a temperature anisotropy are injected continuously into the simulation domain, whose azimuthal drift is determined by a time scale τ_D . Here $\Omega_{e0}\tau_D$ is assumed to be 5,000 in our simulation. The time step is set as $\Omega_{e0}\Delta t = 0.04$ to accurately resolve the electron dynamics.

3. Simulation Results

The whistler-mode waves are excited by temperature anisotropic electrons at the equator, where the amplitudes are quite small. Then, the waves propagate toward polar regions, and their amplitudes become larger and larger until saturate in the latitude range of $\lambda = 10^\circ \sim 15^\circ$ (not shown). To investigate the frequency-time spectrogram of whistler-mode waves, a sliding short-time Fourier analysis has been conducted to fluctuation magnetic field $\delta B_{\perp 1}/B_0$ (where $\delta B_{\perp 1}$ is one perpendicular component of the fluctuating magnetic field), with a time window of 1024 points and a time step of 4 points. Figure 2 describes the power spectral density of $\delta B_{\perp 1}$ at the latitudes of λ = (a) 0° , (b) 5° , (c) 10° , (d) 15° , and (e) 20° . Except at the latitude $\lambda = 0^\circ$, the spectrograms exhibit quasi-monochromatic emissions with three discrete chorus elements, together with a much weaker background whistler-mode wave. The three chirping elements are denoted by the red segment at $\Omega_{e0}t = 5800\text{--}7400$ (element A), the magenta one at $\Omega_{e0}t = 6700\text{--}8400$ (element B), and the blue one at $\Omega_{e0}t = 9500\text{--}11300$ (element C), respectively. The elements A and B have a rising frequency chirping. While element C has a hooked spectrogram: its frequency first increases with time before $\Omega_{e0}t \approx 10200$, and then decreases after $\Omega_{e0}t \approx 10600$. During the propagation from low latitudes (Figure 2b) to higher latitudes (Figure 2e), the hooked spectrogram keeps almost unchanged, except that the wave amplitude gets larger. The discrete and repetitive spectrograms with rising and hooked tones are consistent with those observed in the inner magnetosphere (Figure 1). We will further analyze the typical characteristics of the hooked element in comparison with those of a rising-tone chorus element.

A detailed view of the frequency chirping in the chorus elements has been displayed in Figure 3, where the waveforms of perpendicular fluctuating magnetic field $\delta B_{\perp 1}/B_0$ at $\lambda = 10^\circ$ for (a) element A during $\Omega_{e0}t = 6100\text{--}6900$, and (b) element C during $\Omega_{e0}t = 9500\text{--}11300$ have been shown. The frequency and amplitude of wave circles in both elements are varying with time. To calculate the wave frequencies, the time interval of each wave cycle has been identified, by recording its start and stop time through the zero crossing of $\delta B_{\perp 1}/B_0$ (Tsurutani et al., 2020). The frequencies are the inverse of these time intervals, and have been denoted by blue crosses in Figures 3c and 3d. Note that only the wave cycles with peak amplitudes greater than 0.002 have been shown. The mean frequency values in each $200\Omega_{e0}^{-1}$ interval have also been estimated, which are represented by the black asterisks in the panels with black lines connecting them. During the interval of $\Omega_{e0}t \approx 6220\text{--}6800$ (Figure 3c), the frequencies of element A increase monotonously with time, changing from $\sim 0.25\Omega_{e0}$ to $\sim 0.39\Omega_{e0}$. The corresponding chirping rate in element A is estimated as $\Gamma \approx 2.52 \times 10^{-4}\Omega_{e0}^2$. While the frequencies of electron C

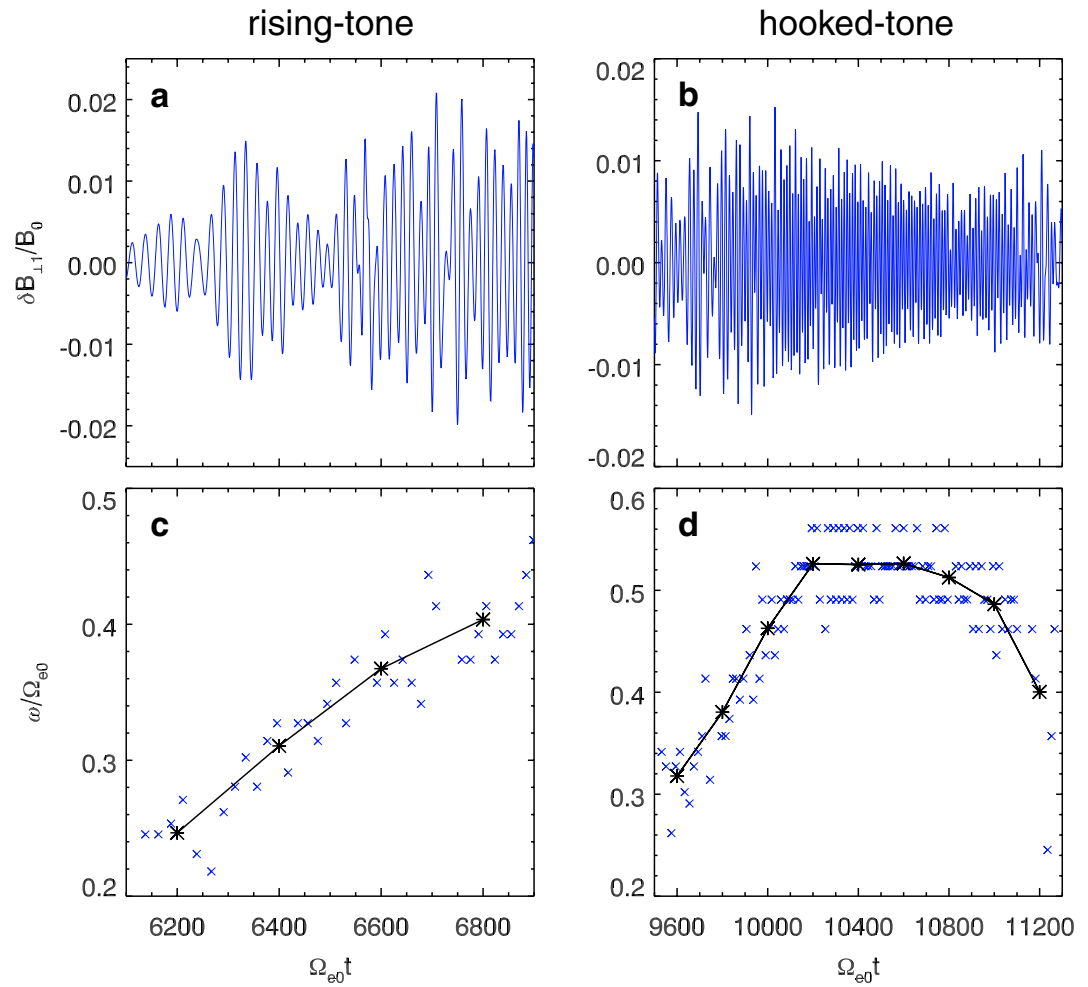


Figure 3. The temporal profile of $\delta B_{\perp 1}$ in (a) element A and (b) element C, and (c) and (d) shows the corresponding wave frequency in each element.

(Figure 3d) first increase with time before $\Omega_{e0}t \approx 10200$ (with a chirping rate of $\Gamma \approx 3.38 \times 10^{-4} \Omega_{e0}^2$), then remain almost unchanged during $\Omega_{e0}t \approx 10200$ – 10600 , and decrease slowly after $\Omega_{e0}t \approx 10600$ (with a chirping rate of $\Gamma \approx -2.01 \times 10^{-4} \Omega_{e0}^2$).

How does the electron phase space density changes along with the excitation of the hooked-tone chorus wave has never been reported before. So, we further analyze the temporal evolution of (a) resonance current J_B and (b) parallel velocity distribution $\delta f(v_{\parallel})/f_0$ around $\lambda = 5^\circ$ in Figure 4. Here, J_B is defined as $J_B = \sum \vec{v} \cdot \delta \vec{B}$ (where \vec{v} is the electron velocity, and $\delta \vec{B}$ is the fluctuating magnetic field), and $\delta f(v_{\parallel})/f_0$ is estimated by using the electrons for $v_{\perp}/V_{Ae} = 2$ – 3 and $\zeta = \pi$ (ζ is the angle between v_{\perp} of electron and wave magnetic field). The time periods when rising-tone and hooked-tone chorus elements appear are denoted by the shadows at $\Omega_{e0}t = 5900$ – 8000 and $\Omega_{e0}t = 9200$ – 10800 in the two panels, respectively. After the excitation of whistler-mode waves at $\Omega_{e0}t \approx 5800$, $\delta f(v_{\parallel})$ has positive values around $v_{\parallel}/V_{Ae} = \pm 2$, which survive till the end of the simulation (Figure 4b). The enhanced phase space density is caused by the pitch angle scattering from perpendicular direction to parallel direction by whistler-mode waves. Along with the generation of two rising-tone elements, there are clear electron holes forming at $v_{\parallel}/V_{Ae} = -1.2 \sim -0.4$ in the phase space, and the corresponding $J_B < 0$ (Figure 4a). This is consistent with theoretical analysis in Nunn (1974) and Omura et al. (2008), which has indicated that the nonlinear interactions between chorus waves and resonant electrons can cause electron holes and negative resonance currents. Interestingly, we find that the electron hole (at $v_{\parallel}/V_{Ae} = -1.0 \sim -0.5$) and negative J_B are also formed when the hooked-tone element appears. The electron holes can be better identified in the v_{\parallel} – ζ space in Figures 4c and 4d), in which the panel (c) is at $\Omega_{e0}t = 9700$ during upward chirping, while the panel (d) is at $\Omega_{e0}t = 10500$

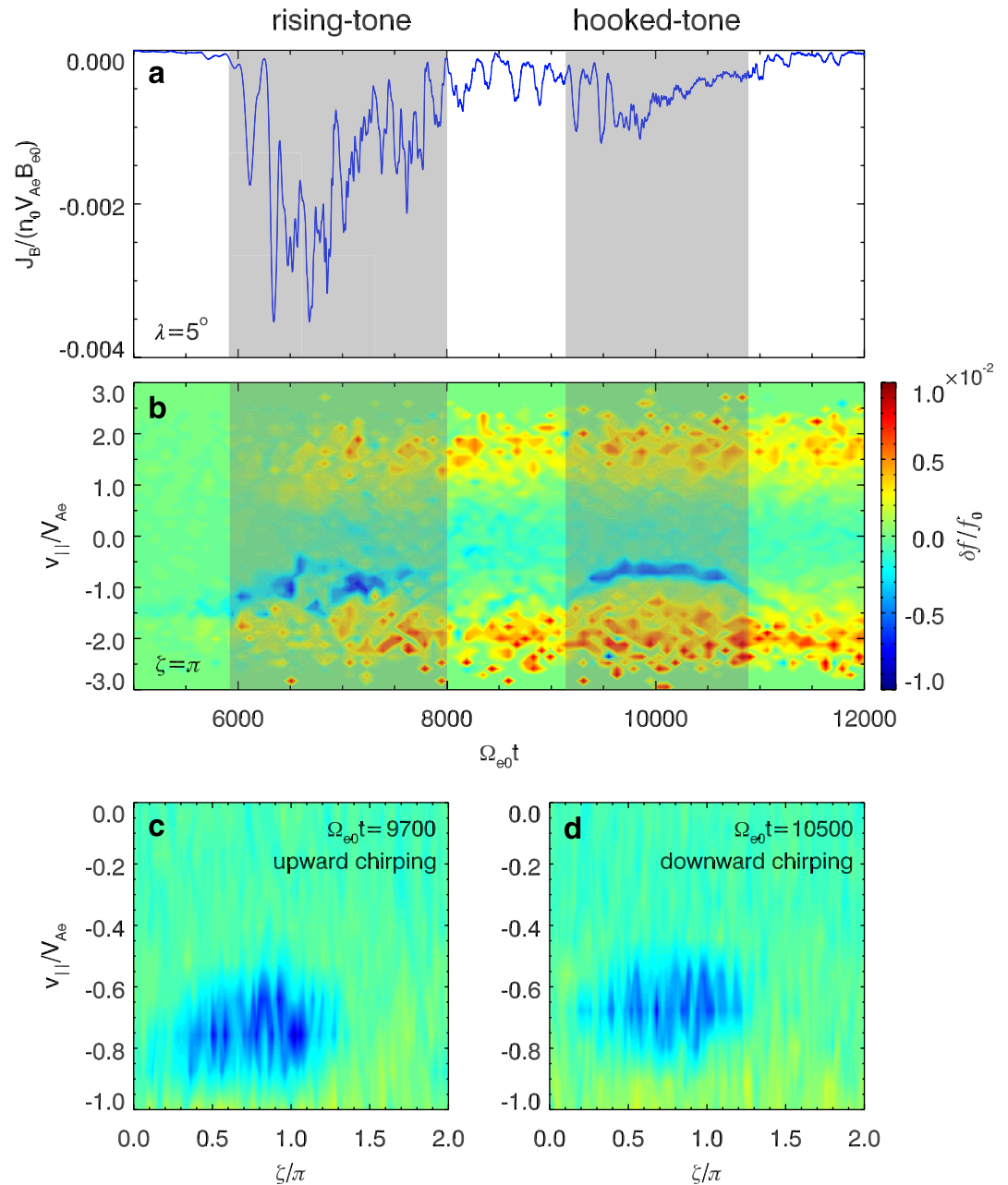


Figure 4. The temporal evolution of (a) resonant current J_B , (b) electron distribution $\delta f(v_{\parallel})/f_0$ at $\zeta = \pi$ and $v_{\perp}/V_{Ae} = 2-3$. The distributions of $\delta f(v_{\parallel})/f_0$ in the ζ - v_{\parallel} space at (c) $\Omega_{e0} t = 9700$ and (d) $\Omega_{e0} t = 10500$.

during downward chirping. As shown in both panels, the number density of trapped electrons inside the resonant island is much lower than that of the surrounding untrapped electrons, indicating that the electron hole is formed no matter whether the wave frequency is upward chirping or downward chirping.

4. Conclusions and Discussion

With a 1-D gcPIC- δf simulation in a dipole magnetic field, we investigate the repetitive chorus emissions in the Earth's inner magnetosphere, excited by energetic electrons with a temperature anisotropy. The chorus waves contain a series of discrete elements with frequency chirpings when they leave away from the equator. Along with two rising-tone elements, we identify one element with a hooked spectrogram, whose frequency first increases

with time, and then decreases. This is consistent with satellite observations, which have shown that there is occasionally one or several hooked-tone spectrograms combined with rising-tone elements (Figure 1). Furthermore, we find that the electron holes occur simultaneously with the formation of both rising-tone and hooked-tone chorus elements.

The generation mechanism of chorus frequency chirping has been widely investigated in previous studies (Katoh & Omura, 2011; Ke et al., 2020; Nunn, 1974; Omura et al., 2008; Q. Lu et al., 2019; Tao, 2014). Theoretical studies have shown that the nonlinear interactions between whistler-mode waves and resonant electrons can produce electron holes or hills in the phase space (Nunn, 1974; Omura et al., 2008). The electron holes can cause upward chirping due to negative resonant currents, while a downward chirping is driven by electron hills and positive currents. This has been further supported by numerical simulations, in which the electron holes (Nunn & Omura, 2015; Tao et al., 2017) or hills (Nunn & Omura, 2012; Nogi & Omura, 2021; Nogi et al., 2020) are formed. By pumping a triggering wave at the equator, Nogi et al. (2020) and Nogi and Omura (2021) have produced the downward frequency chirping and electron hills in the phase space, which is consistent with the theoretical predictions proposed by Nunn (1974) and Omura et al. (2008). While in our simulation, the waves are self-consistently excited by anisotropic electrons, exhibiting an upward chirping followed by a downward chirping (known as a hooked spectrogram). When the downward chirping appears, there are clear electron holes formed, and the corresponding resonance currents are negative (Figure 4). This cannot be well accounted for by the current theoretical model of chorus waves, which may invoke a new theoretical model for the excitation of hooked chorus waves, or even for both the rising-tone and falling-tone chorus waves. Moreover, our study presents an important clue that the electron hole may also produce the falling-tone chorus element, providing a novel idea for theoretical analysis.

Data Availability Statement

The simulation data are archived in <https://dx.doi.org/10.12176/01.99.01727>.

Acknowledgments

This work was supported by the Strategic Priority Research Program of Chinese Academy of Sciences Grant Nos. XDB41000000, Key Research Program of Frontier Sciences CAS (QYZDJ-SSW-DQC010), USTC Research Funds of the Double First-Class Initiative (YD3420002001), the Fundamental Research Funds for the Central Universities (WK3420000013), and “USTC Tang Scholar” program. We acknowledge the entire Van Allen Probes instrument group. We also acknowledge for the data resource from “National Space Science Data Center, National Science & Technology Infrastructure of China (<http://www.nssdc.ac.cn>).”

References

- Burtis, W. J., & Helliwell, R. A. (1969). Banded chorus a new type of VLF radiation observed in the magnetosphere by OGO 1 and OGO 3. *Journal of Geophysical Research*, 74(11), 3002–3010. <https://doi.org/10.1029/ja074i011p03002>
- Chen, H., Gao, X., Lu, Q., Ke, Y., & Wang, S. (2017). Lower band cascade of whistler waves excited by anisotropic hot electrons: One-dimensional PIC simulations. *Journal of Geophysical Research: Space Physics*, 122(10), 10448–10457. <https://doi.org/10.1002/2017JA024513>
- Chen, H., Gao, X., Lu, Q., Sauer, K., Chen, R., Yao, J., & Wang, S. (2021). Gap formation around $0.5\Omega_e$ of whistler-mode waves excited by electron temperature anisotropy. *Journal of Geophysical Research: Space Physics*, 126(2). <https://doi.org/10.1029/2020JA028631>
- Helliwell, R. A. (1967). A theory of discrete VLF emissions from the magnetosphere. *Journal of Geophysical Research*, 72, 4773–4790. <https://doi.org/10.1029/jz072i019p04773>
- Hikishima, M., Yagitani, S., Omura, Y., & Nagano, I. (2009). Full particle simulation of whistler-mode rising chorus emissions in the magnetosphere. *Journal of Geophysical Research*, 114, A01203. <https://doi.org/10.1029/2008JA013625>
- Horne, R. B., & Thorne, R. M. (1998). Potential waves for relativistic electron scattering and stochastic acceleration during magnetic storms. *Geophysical Research Letters*, 25(15), 3011–3014. <https://doi.org/10.1029/98GL01002>
- Horne, R. B., Thorne, R. M., Meredith, N. P., & Anderson, R. R. (2003). Diffuse auroral electron scattering by electron cyclotron harmonic and whistler mode waves during an isolated substorm. *Journal of Geophysical Research*, 108(A7), 1290. <https://doi.org/10.1029/2002JA009736>
- Hu, G., & Krommes, J. A. (1994). Generalized weighting scheme for δf particle-simulation method. *Physics of Plasmas*, 1(4), 863–874. <https://doi.org/10.1063/1.870745>
- Katoh, Y., & Omura, Y. (2011). Amplitude dependence of frequency sweep rates of whistler mode chorus emissions. *Journal of Geophysical Research*, 116, A07201. <https://doi.org/10.1029/2011JA016496>
- Ke, Y., Gao, X., Lu, Q., Wang, X., & Wang, S. (2017). Generation of rising tone chorus in a two-dimensional mirror field by using the general curvilinear PIC code. *Journal of Geophysical Research: Space Physics*, 122, 8154–8165. <https://doi.org/10.1002/2017JA024178>
- Ke, Y., Lu, Q., Gao, X., Wang, X., Chen, L., Wang, S., & Wang, S. (2020). Particle-in-cell simulations of characteristics of rising-tone chorus waves in the inner magnetosphere. *Journal of Geophysical Research: Space Physics*, 125, e2020JA027961. <https://doi.org/10.1029/2020JA027961>
- Kennel, C. F., & Petschek, H. E. (1966). Limit on stable trapped particle fluxes. *Journal of Geophysical Research*, 71(1), 1–28. <https://doi.org/10.1029/JZ071i001p00001>
- Lorentzen, K. R., Blake, J. B., Inan, U. S., & Bortnik, J. (2001). Observations of relativistic electron microbursts in association with VLF chorus. *Journal of Geophysical Research*, 106(A4), 6017–6027. <https://doi.org/10.1029/2000JA003018>
- Lu, Q., Chen, L., Wang, X., Gao, X., Lin, Y., & Wang, S. (2021). Repetitive emissions of rising-tone chorus waves in the inner magnetosphere. *Geophysical Research Letters*, 48, e2021GL094979. <https://doi.org/10.1029/2021GL094979>
- Lu, Q., Ke, Y., Wang, X., Liu, K., Gao, X., Chen, L., & Wang, S. (2019). Two-dimensional general curvilinear particle-in-cell (gcPIC) simulation of rising-tone chorus waves in a dipole magnetic field. *Journal of Geophysical Research: Space Physics*, 124, 4157–4167. <https://doi.org/10.1029/2019ja026586>
- Lu, Q. M., Wang, L. Q., Zhou, Y., & Wang, S. (2004). Electromagnetic instabilities excited by electron temperature anisotropy. *Chinese Physics Letters*, 21, 129–132.

- Meredith, N. P., Horne, R. B., & Anderson, R. R. (2001). Substorm dependence of chorus amplitudes: Implications for the acceleration of electrons to relativistic energies. *Journal of Geophysical Research*, 106(A7), 13165–13178. <https://doi.org/10.1029/2000JA900156>
- Nishimura, Y., Bortnik, J., Li, W., Thorne, R. M., Ni, B., Lyons, L. R., et al. (2013). Structures of dayside whistler-mode waves deduced from conjugate diffuse aurora. *Journal of Geophysical Research: Space Physics*, 118, 664–673. <https://doi.org/10.1029/2012ja018242>
- Nogi, T., Nakamura, S., & Omura, Y. (2020). Full particle simulation of whistler-mode triggered falling-tone emissions in the magnetosphere. *Journal of Geophysical Research: Space Physics*, 125, e2020JA027953. <https://doi.org/10.1029/2020JA027953>
- Nogi, T., & Omura, Y. (2021). Nonlinear signatures of VLF-triggered emissions: A simulation study. *Journal of Geophysical Research: Space Physics*, 127, e2021JA029826. <https://doi.org/10.1029/2021JA029826>
- Nunn, D. (1974). A self-consistent theory of triggered VLF emissions. *Planet. Space Sci.*, 22, 349–378. [https://doi.org/10.1016/0032-0633\(74\)90070-1](https://doi.org/10.1016/0032-0633(74)90070-1)
- Nunn, D., & Omura, Y. (2012). A computational and theoretical analysis of falling frequency VLF emissions. *Journal of Geophysical Research*, 117, A08228. <https://doi.org/10.1029/2012JA017557>
- Nunn, D., & Omura, Y. (2015). A computational and theoretical investigation of nonlinear wave-particle interactions in oblique whistlers. *Journal of Geophysical Research: Space Physics*, 120, 2890–2911. <https://doi.org/10.1002/2014JA020898>
- Nunn, D., Omura, Y., Matsumoto, H., Nagano, I., & Yagitani, S. (1997). The numerical simulation of VLF chorus and discrete emissions observed on the Geotail satellite using a Vlasov code. *Journal of Geophysical Research*, 102(A12), 27083–27097. <https://doi.org/10.1029/97ja02518>
- Omura, Y., Katoh, Y., & Summers, D. (2008). Theory and simulation of the generation of whistler-mode chorus. *Journal of Geophysical Research*, 113, A04223. <https://doi.org/10.1029/2007JA012622>
- Omura, Y., Nakamura, S., Kletzing, C. A., Summers, D., & Hikishima, M. (2015). Nonlinear wave growth theory of coherent hiss emissions in the plasmasphere. *J. Geophys. Res. Space Physics*, 120, 7642–7657. <https://doi.org/10.1002/2015JA021520>
- Parker, S. E., & Lee, W. W. (1993). A fully nonlinear characteristic method for gyrokinetic simulation. *Physics of Fluids B*, 5(1), 77–86. <https://doi.org/10.1063/1.860870>
- Pickett, J. S., Santolík, O., Kahler, S. W., Masson, A., Adrian, M. L., Gurnett, D. A., et al. (2005). Multi-point cluster observations of VLF Risers, Fallers and hooks at and near the plasmapause. In J. A. Sauvaud, & Z. Němeček (Eds.), *Multiscale processes in the Earth's magnetosphere: From interball to cluster*. NATO Science series II: Mathematics, physics and chemistry (Vol. 178, pp. 307–328). Springer. https://doi.org/10.1007/1-4020-2768-0_17
- Santolík, O., & Gurnett, D. A. (2003). Transverse dimensions of chorus in the source region. *Geophysical Research Letters*, 30(2), 1031. <https://doi.org/10.1029/2002GL016178>
- Summers, D., Omura, Y., Miyashita, Y., & Lee, D. H. (2012). Nonlinear spatiotemporal evolution of whistler mode chorus waves in Earth's inner magnetosphere. *Journal of Geophysical Research*, 117, A09206. <https://doi.org/10.1029/2012ja017842>
- Summers, D., Thorne, R. M., & Xiao, F. L. (1998). Relativistic theory of wave-particle resonant diffusion with application to electron acceleration in the magnetosphere. *Journal of Geophysical Research*, 103(A9), 20487–20500. <https://doi.org/10.1029/98JA01740>
- Sydora, R. D. (2003). In J. Buchner, C. T. Dum, & M. Scholer (Eds.), *Low noise electrostatic and electromagnetic δf particle-in-cell simulation of plasmas*. *Space Plasma Simulation* (pp. 109–124). LNP 615.
- Tao, X. (2014). A numerical study of chorus generation and the related variation of wave intensity using the DAWN code. *J. Geophys. Res. Space Physics*, 119, 3362–3372. <https://doi.org/10.1002/2014JA019820>
- Tao, X., Zonca, F., & Chen, L. (2017). Investigations of the electron phase space dynamics in triggered whistler wave emissions using low noise δf method. *Plasma Physics and Controlled Fusion*, 59, 094001. <https://doi.org/10.1088/1361-6587/aa759a>
- Thorne, R. M., Ni, B., Tao, X., Horne, R. B., & Meredith, N. P. (2010). Scattering by chorus waves as the dominant cause of diffuse auroral precipitation. *Nature*, 467(7318), 943–946. <https://doi.org/10.1038/nature09467>
- Tsurutani, B. T., Chen, R., Gao, X., Lu, Q., Pickett, J. S., Lakhina, G. S., et al. (2020). Lower-band “monochromatic” chorus riser subelement/wave packet observations. *Journal of Geophysical Research: Space Physics*, 125, e2020JA028090. <https://doi.org/10.1029/2020JA028090>
- Tsurutani, B. T., & Smith, E. J. (1974). Postmidnight chorus: A substorm phenomenon. *Journal of Geophysical Research*, 79(1), 118–127. <https://doi.org/10.1029/JA079i001p00118>
- Tsurutani, B. T., & Smith, E. J. (1977). Two types of magnetospheric ELF chorus and their substorm dependences. *Journal of Geophysical Research*, 82(32), 5112–5128. <https://doi.org/10.1029/JA082i032p05112>
- Turner, D. L., Lee, J. H., Claudepierre, S. G., Fennell, J. F., Blake, J. B., Jaynes, A. N., Santolík, O., et al. (2017). Examining coherency scales, substructure, and propagation of whistler mode chorus elements with Magnetospheric Multiscale (MMS). *Journal of Geophysical Research: Space Physics*, 122(11), 11201–11226. <https://doi.org/10.1002/2017JA024474>